# Exciton Absorption Spectra by Linear Response Methods: Application to Conjugated Polymers

Martín A. Mosquera,[†] Nicholas E. Jackson,[†,‡] Thomas J. Fauvell,[†] Matthew S. Kelley,[†] Lin X. Chen,[†,‡] George C. Schatz,[†] and Mark A. Ratner*[,†]

[†]Department of Chemistry and the Materials Research Center, Northwestern University, 2145 Sheridan Road, Evanston, Illinois 60208, United States

[‡]Chemical Sciences and Engineering Division, Argonne National Laboratory, 9700 South Cass Avenue, Lemont, Illinois 60439, United States

**S** Supporting Information

**ABSTRACT:** The theoretical description of the time-evolution of excitons requires, as an initial step, the calculation of their spectra, which has been inaccessible to most users due to the high computational scaling of conventional algorithms and accuracy issues caused by common density functionals. Previously (*J. Chem. Phys.* **2016**, *144*, 204105), we developed a simple method that resolves these issues. Our scheme is based on a two-step calculation in which a linear-response TDDFT calculation is used to generate orbitals perturbed by the excitonic state, and then a second linear-response TDDFT calculation is used to determine the spectrum of excitations relative to the excitonic state. Herein, we apply this theory to study near-infrared absorption spectra of excitons in oligomers



of the ubiquitous conjugated polymers poly(3-hexylthiophene) (P3HT), poly(2-methoxy-5-(2-ethylhexyloxy)-1,4-phenylenevinylene) (MEH-PPV), and poly(benzodithiophene-thieno[3,4-*b*]thiophene) (PTB7). For P3HT and MEH-PPV oligomers, the calculated intense absorption bands converge at the longest wavelengths for 10 monomer units, and show strong consistency with experimental measurements. The calculations confirm that the exciton spectral features in MEH-PPV overlap with those of the bipolaron formation. In addition, our calculations identify the exciton absorption bands in transient absorption spectra measured by our group for oligomers (1, 2, and 3 units) of PTB7. For all of the cases studied, we report the dominant orbital excitations contributing to the optically active excited state—excited state transitions, and suggest a simple rule to identify absorption peaks at the longest wavelengths. We suggest our methodology could be considered for further developments in theoretical transient spectroscopy to include nonadiabatic effects, coherences, and to describe the formation of species such as charge-transfer states and polaron pairs.
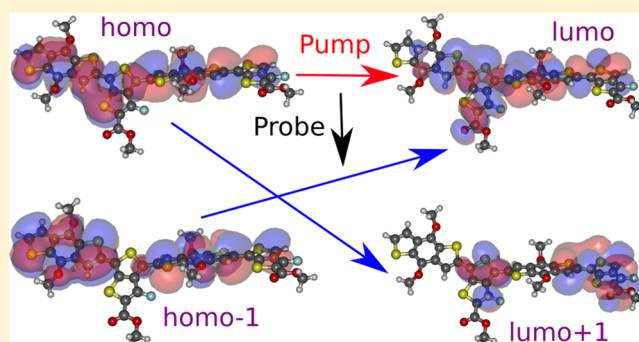
## INTRODUCTION

The spectroscopic analysis of photoinduced charge generation usually begins with the assignment of photon wavelengths at which excitons predominantly absorb.[1,2] In conjugated polymers, this is particularly vital, as inhomogeneous broadening in both solutions and films often leads to shapeless excited-state absorption (ESA) spectra. Accurate peak identification allows for differentiation of excitons from other species such as bipolarons, free polarons, and charge-transfer states, simplifying the monitoring of photophysical dynamics. While researchers typically rely upon correlating kinetics between peaks, or simple external controls (spectroelectrochemistry, $O_2$ quenching, applied magnetic fields, temperature variations) for peak assignment, the application of theoretical methods for peak identification in transient spectroscopy has been severely limited to date.[3−5] Although there are many productive theoretical models for excited-state phenomena in general, the development of inexpensive first-principles quantum

chemical methods is still a challenging goal. DFT-based methodologies are becoming remarkably accurate for ground-state properties, due to the development of robust exchange-correlation density functionals such as those from the Minnesota[6] and meta-GGA families.[7] However, TDDFT functional development and application are very sensitive, and involve a significant amount of details and restrictions to accurately describe time-dependent electronic phenomena.[8,9]

Algorithms developed within quadratic response (QR) TDDFT and correlated wave function theories are able to compute ESA and two-photon absorption cross sections.[10−12] The main advantage of correlated wave function quadratic theories is that the user can obtain highly accurate results. However, the computational demands are significantly higher than those in standard linear response (LR) methods. For

instance, QR TDDFT calculations, roughly speaking, scale as $N^6$, whereas LR TDDFT computations scale as $N^4$. For calculation of the absorption spectrum of a given excited state, ref 4 presents a promising real-time TDDFT method that consists of generating an approximation to the excited state of interest, and then propagating and analyzing this excited state. During the propagation in this method, the time-dependent exchange-correlation potential reduces accuracy by red-shifting the excitation energies for transitions starting from the excited state of interest; this peak-shifting problem also arises in QR TDDFT. Over-relaxation of excitation energies is common in real-time propagations.[13−16] Moreover, even though real-time propagation techniques are powerful, their straightforward application is limited outside of theoretically focused research groups, making the incorporation of real-time methods into the toolbox of spectroscopic analysis, as is the case for standard ground-state TDDFT, unlikely at present.

We recently proposed a second linear-response (SLR) algorithm (described in the following section) and a formalism based on wave function theory and LR TDDFT to estimate excited-state absorption spectra.[17] For a given molecular geometry, the SLR method outputs the oscillator strengths for transitions from an excited state chosen by the user. In principle, other quantities such as excited state−excited state transition densities can be calculated as well. The SLR algorithm avoids over-relaxation of excitation energies, and the total computational cost is only twice that of a regular LR calculation. The method was successfully applied to estimate transient absorption spectra in the X-ray and UV/vis regimes. In this Article, we utilize the SLR method to help resolve the common predicament of excited-state transient spectra prediction for large oligomeric systems. We demonstrate that SLR accurately describes the exciton absorption spectra of two canonical conjugated polymers, via the analysis of the ESA of their oligomers (Scheme 1): poly(phenylene-vinylene) (MEH-

**Scheme 1. Molecular Structures Considered in This Work**
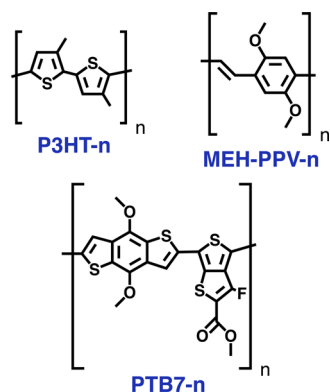


PPV) ($n = 2,4,6,8,10$) and poly(3-hexylthiophene) (P3HT) ($n = 2,4,6,8,10$). Our calculations confirm experimental exciton line shape assignments for the polymers P3HT and MEH-PPV. In addition, we apply SLR to describe the exciton absorption profiles of three ($n = 1,2,3$) oligomers of poly-(benzodithiophene-thieno[3,4-$b$]thiophene) (PTB7), a more recent "donor−acceptor" conjugated polymer known for being a champion organic photovoltaic material. We include oligomer-specific transient absorption spectra measured by our group that validate our computational predictions. For the systems studied in this work, the nature of the dominant

molecular orbitals contributing to the highest oscillator strength ESA transitions from the $S_1$ state is explicitly identified, and the conjugation length dependence of these transitions is determined. It is our hope that this demonstration of the computationally efficient SLR technique over a chemically diverse set (with atoms such as S, F, and O) of organic semiconducting materials serves as motivation for its standard incorporation into the common computational toolkits of transient optical spectroscopists.

## ■ THEORY

We denote the many-body eigenfunctions of the system as $\{\Psi_K\}$. These wave functions satisfy $\hat{H}\Psi_K = E_K\Psi_K$, where $\hat{H}$ is the Hamiltonian describing the electronic degrees of freedom of the molecule. The ground-state wave function is $\Psi_0$. Traditionally, perturbation theory approaches assume that the system is initially in the ground state ($\Psi_0$), and then a weak external perturbation is turned on. In our case, we are interested in describing how a system in the excited state $\Psi_I$ transitions into other states. To achieve this, we performed a perturbation theory analysis for a different initial state,[17] in which the ground state is slightly perturbed by the excited state $\Psi_I$. This initial state is $\Psi_0 + \lambda\Psi_I$, where $\lambda > 0$. We showed that the residues of the polarizability tensor (in frequency space) of the system provide the perturbed dipole vector $\mathbf{d}_{JI}(\lambda) = \langle\Psi_J|\hat{\boldsymbol{\mu}}|\Psi_0 + \lambda\Psi_I\rangle$, which upon differentiation with respect to $\lambda$ gives the oscillator strength of the $I \rightarrow J$ transition: $f_{JI} = 2/3\Omega_{JI}|\langle\Psi_J|\hat{\boldsymbol{\mu}}|\Psi_I\rangle|^2$, where $\Omega_{JI} = E_J - E_I$.

Scheme 2 summarizes the steps required to compute $\{f_{JI}\}$ within linear-response TDDFT. The algorithm to calculate the

**Scheme 2. Diagram Summarizing the Procedure To Calculate an ESA Spectrum**[a]
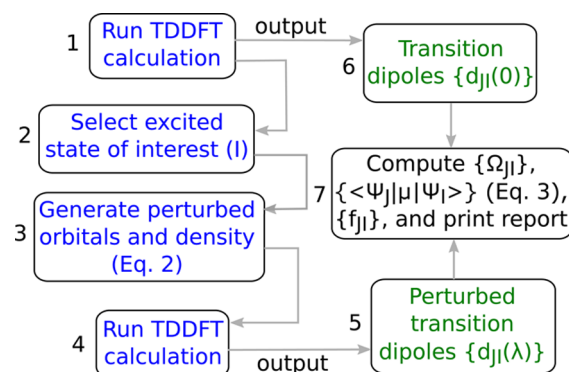


[a]The oscillator strength of an excited state−excited state transition is computed as $f_{JI} = 2/3\Omega_{JI}|\langle\Psi_J|\hat{\boldsymbol{\mu}}|\Psi_I\rangle|^2$, where $\Omega_{JI}$ is the frequency of the $I \rightarrow J$ transition. The frequencies $\{\Omega_{JI}\}$ are computed using data from the original LR spectrum (first step shown above), $\Omega_{JI} = \Omega_J - \Omega_I$. Each transition dipole vector $\langle\Psi_J|\hat{\boldsymbol{\mu}}|\Psi_I\rangle$ is calculated using first-order finite differences, eq 3, where $\lambda$ is a number close to zero.

absorption spectrum of an excited state is as follows: (i) Perform a standard linear-response TDDFT calculation. (ii) Select the excited state of interest, and perturb the ground-state orbitals. (iii) Run a new linear-response calculation with reference to the perturbed orbitals. (iv) By comparing the transition dipoles from the two LR calculations, the absorption spectrum of the excited state of interest is calculated, as we explain below.

In the traditional LR approach, one solves the Casida, or random phase approximation equations:

$$\begin{pmatrix} \mathbf{A} & \mathbf{B} \\ \mathbf{B} & \mathbf{A} \end{pmatrix} \begin{pmatrix} \mathbf{X} \\ \mathbf{Y} \end{pmatrix} = \Omega \begin{pmatrix} 1 & 0 \\ 0 & -1 \end{pmatrix} \begin{pmatrix} \mathbf{X} \\ \mathbf{Y} \end{pmatrix} \tag{1}$$

The matrices $\mathbf{A}$ and $\mathbf{B}$ depend on the ground-state electronic density of the system, which is determined by the ground-state orbitals, denoted here as $\{\psi_p\}$. We use the index $i$ for occupied orbitals, and $a$ for unoccupied ones. The vectors $\mathbf{X}$ and $\mathbf{Y}$ are quantities required to compute the electronic transition densities of the system. For each excited state, $K$, there is a pair of vectors $\mathbf{X}^K$, $\mathbf{Y}^K$ and excitation frequency $\Omega_K = E_K - E_0$. The initial state $\Psi_0 + \lambda\Psi_I$ is represented here by the perturbed orbitals (second step of the algorithm):

$$\tilde{\psi}_i(\mathbf{r}) = \psi_i(\mathbf{r}) + \lambda \sum_a (X_{ai}^I + Y_{ai}^I)\psi_a(\mathbf{r}) \tag{2}$$

These orbitals ($\{\tilde{\psi}_i\}$) reproduce the initial density of the perturbed system, up to first order in $\lambda$. Using the new orbitals ($\{\tilde{\psi}_p\}$), we run again the linear-response calculations. This step does not require alteration of the standard LR TDDFT algorithm: The routine that solves the Casida equations only needs the new set of orbitals $\{\tilde{\psi}_p\}$ (or eigenvectors), and then the user requests that the program solves the Casida equations once more. Let us denote $\{\mathbf{d}_J^0 = \langle\Psi_J|\hat{\boldsymbol{\mu}}|\Psi_0\rangle\}$ as the set of transition dipoles obtained from the first LR problem. We approximate the transition element $\langle\Psi_J|\hat{\boldsymbol{\mu}}|\Psi_I\rangle$ by numerical differentiation:

$$\langle\Psi_J|\hat{\mu}|\Psi_I\rangle \approx \frac{\mathbf{d}_{JI}(\lambda) - \mathbf{d}_J^0}{\lambda} \tag{3}$$

The perturbed transition dipoles $\mathbf{d}_{JI}$ are printed out after running the LR TDDFT calculations for the second time using the orbitals shown in eq 2. In principle, as $\lambda \to 0$, the frequencies from the SLR and LR calculations get progressively closer. This eliminates the peak-shifting problem mentioned in the first section, and allows us to calculate $\Omega_{JI}$ using the excitation energies from the first LR calculation, that is, $\Omega_{JI} = \Omega_J - \Omega_I$.

We selected $n$-repeat unit oligomers of P3HT ($n$ = 2,4,6,8,10), PTB7 ($n$ = 1,2,3), and MEH-PPV ($n$ = 2,4,6,8,10), and carried out geometry optimizations with the exchange-correlation (XC) functional PBE[18] and the basis set 6-31G* (Figures S1−3).[19] The oligomer size selection for P3HT and MEH-PPV is supported by the work of Risko et al.,[20] who showed that the frontier orbitals delocalize on a range of up to 10 contiguous aromatic rings. We refer to a given oligomer by the abbreviation of the corresponding polymer, followed by the number of units used. For example, P3HT-2 is an oligomer with two repeat units. Typically the conjugated polymers possess pendant alkyl side-chains to enhance solubility, but we utilize the common literature approximation of cleaving the side-chains to a terminal methyl group, which has little to no effect on the valence orbitals;[20] the structures shown in Scheme 1 may be considered the exact structures modeled. These geometries were then used as input for subsequent excited-state calculations. For each oligomer at its optimal geometry, we ran a standard LR TDDFT calculation to generate the lowest-lying, high-oscillator strength exciton state, here denoted S$_1$. The transition vectors resulting from the calculation of the S$_1$ state were then used to perform the second LR estimations. The molecules in real experimental conditions

are surrounded by random environments. This is reflected by a disordered distribution of molecular geometries. Equilibrium geometries from any proper density-functional for the isolated molecule, including the exact one, are assumed to yield a representative configuration of the ensemble of all of the likely geometries. Hence, for simplicity, we use PBE geometries.

CAM-LDA0 is the XC functional employed for the excited-state calculations. The exchange energy in CAM-LDA0 is split into 25% global and 50% long-range Hartree−Fock exchange, 25% global and 50% short-range LDA exchange energies,[21] and 100% LDA correlation.[22] To verify the exchange percentages are correct, note that the long- and short-range exchange energies must be first factorized as 50% (long-range + short-range), which then amounts to 50% of the global exchange in the uniform electron gas limit. Adding this to 25% of nonlocal exchange and 25% LDA exchange, in the uniform electron gas limit, we recover 100% exchange energy. With respect to CAM-B3LYP[23,24] or CAM-PBE0,[25] LR TDDFT computations with CAM-LDA0 are twice as fast, and yield very similar excitation energies (within 0.2 eV) and oscillator strengths for charge-transfer, Rydberg, and local excitations.[26] The positive applicability of CAM XC functionals to $\pi$-conjugated fluorene oligomers has been demonstrated previously by Ling et al.[3] Because only excitations of relatively short-range (not Rydberg-like) are required, we use the cc-pVDZ basis set[27] for the LR calculations, except for PTB7-3 and MEH-PPV-10, which were studied with the SBKJC VDZ basis set and its effective core potential[28] (this set reduces computational costs and gives results similar to those of cc-pVDZ).

All of the calculations discussed in this work, including SLR, were performed with the NWChem computational package,[29] and using the random phase approximation (RPA); in other words, the "Y" vectors were always computed. In our experience, CAM-LDA0 calculations with RPA tend to be more accurate than those with the Tamm−Dancoff approximation (i.e., ignoring "Y" vectors). The excited state−excited state transition dipoles $\{\langle\Psi_J|\hat{\boldsymbol{\mu}}|\Psi_I\rangle\}$ are calculated by means of first-order finite differences, eq 3, which approximate the derivative of $\mathbf{d}_{JI}(\lambda)$ around $\lambda = 0$. Once these transition dipoles are estimated, the SLR algorithm computes the oscillator strengths ($f_{JI} = 2/3\Omega_{JI}|\langle\Psi_J|\hat{\boldsymbol{\mu}}|\Psi_I\rangle|^2$).

After resolving the Casida equation for perturbed initial orbitals (step 4, Scheme 2), a new set of excitation vectors is produced; we denote this set as $\{\tilde{\mathbf{X}}^J, \tilde{\mathbf{Y}}^J\}$. These vectors are required to compute the perturbed transition dipoles. Because the perturbation alters the ordering of this set of vectors with respect to the original arrangement, the SLR algorithm relabels the vectors so the correct dipoles are compared in the computation of the numerical derivatives, eq 3. The relabeling criterion used by the algorithm is as follows:[17] Two pairs of excitation vectors $(\mathbf{X}^J, \mathbf{Y}^J)$ and $(\tilde{\mathbf{X}}^K, \tilde{\mathbf{Y}}^K)$ correspond to one another if $1 - C_{\text{tol}} < |(\mathbf{X}^J)^T\tilde{\mathbf{X}}^K - (\mathbf{Y}^J)^T\tilde{\mathbf{Y}}^K| < 1 + C_{\text{tol}}$, where $C_{\text{tol}}$ is a number close to zero chosen by the user, and the superscript "$T$" indicates transpose. If the criterion is met, then the algorithm replaces the label $K$ by $J$. Once the labels are properly reassigned, the SLR algorithm computes $\mathbf{d}_{JI}$, using $(\tilde{\mathbf{X}}^J, \tilde{\mathbf{Y}}^J)$, and proceeds with computing the numerical derivatives.

Numerical differentiation, to estimate excited state−excited state transition dipoles, demands $\lambda$ be a number close to zero. Under (costumary) small trial vector spaces and moderate convergence criteria, very small values leave in general the shape of the spectrum unaffected, but might cause few oscillator strengths to be unphysically too large. To avoid this, we

progressively increase the value of $\lambda$ until large variations in the oscillator strengths disappear. We consider the oligomer P3HT-2 as reference. We compute the absorption spectrum of the $S_1$ state for several candidate values of $\lambda$: 0.01, 0.05, 0.1, and 0.2. Here, we use the values $C_{tol} = 0.005$ and 0.01 for $\lambda = 0.01$ and 0.05, respectively; for $\lambda = 0.1$ and $\lambda = 0.2$, we use $C_{tol} = 0.05$. Values of $\lambda$ greater than 0.2 make the relabeling more difficult because the inner products differ significantly from unity. Hence, we stop at $\lambda = 0.2$. Figure S1 shows that the spectra in the range of interest are similar for the candidate values of $\lambda$ tested. We choose $\lambda = 0.1$ because for this value the oscillator strengths are also well behaved in the range 350−550 nm.

## ■ EXPERIMENTAL METHOD

Transient absorption measurements were performed on PTB7 oligomers in chloroform solution using a Coherent ultrafast laser system. The system includes a Ti:sapphire oscillator (Mira) pumped by a diode laser (Verdi-5), a regenerative amplifier (RegA 9050) pumped by its own diode laser (Verdi-10), a separate stretcher/compressor, and an optical parametric amplifier (OPA, Coherent). The amplified output of the RegA (10 $\mu$J/pulse at 100 kHz repetition rate) was compressed to close to 50 fs and then divided with an 80/20 beam splitter. The low power split fundamental beam was tightly focused on a 3 mm thick sapphire plate to generate the near-IR probe beam signal in the spectral range of 850−1670 nm, while the higher power beam was used to pump the OPA to generate the excitation pulse. The IR signal was spectrally dispersed with a monochromator (Princeton Instruments Acton SP2300) and detected with a liquid nitrogen cooled CCD array (Princeton Instruments Pylon IR).

## ■ RESULTS AND DISCUSSION

For each oligomer, we calculated the oscillator strengths of $S_1 \rightarrow S_n$ transitions using the SLR algorithm and broadened these values with Gaussian functions. To compare the computed spectra against the experimental ones, for each system we scaled all of the oscillator strengths of each oligomer by the same single factor; the relative heights are preserved. The Gaussian bandwidth ($\sigma$) we use is 50 nm and applied for all of the computed solid lines. This is designed to mimic bandwidths that could be obtained by more rigorous methods such as ab initio molecular dynamics.

In Figure 1 we show the computed versus experimental ESA spectra for P3HT. The experimental data measured by Guo et al.[30] for exciton absorption of regiorandom P3HT are included. The pump wavelength is 400 nm, power density around 30 $\mu$J/cm$^2$, and pump−probe delay is 0 ps. Regiorandom P3HT forms
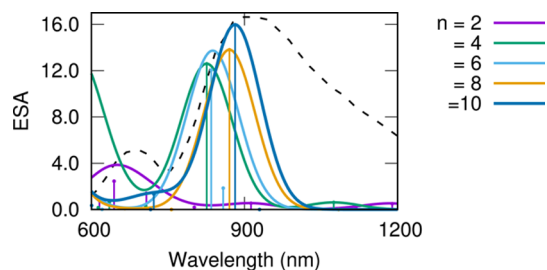


**Figure 1.** $S_1$ absorption spectra of P3HT oligomers. The dashed and solid lines represent experimental data[30] and broadened calculated absorption strengths, respectively. The vertical lines indicate positioning of the excitation energies of transitions from the $S_1$ state, and are proportional to the heights of the discrete oscillator strengths of these transitions. The solid lines were broadened with Gaussian functions ($\sigma$ = 50 nm).

disordered polymer chains, favoring more localized excitons than in regioregular P3HT. Guo et al.[30] assigned the band around 900 nm to absorption by the exciton state because it vanishes 100 ps after excitation, while the stimulated emission signal decays similarly. The small peak around 700 nm is due to bipolarons, as confirmed by transient anisotropy measurements.

The initial LR TDDFT calculations indicate $S_0 \rightarrow S_1$ is the main transition among the low-lying possible excitations. For the oligomer P3HT with 10 units, the wavelength of the $S_0 \rightarrow S_1$ transition is 521 nm, in agreement with the peak at 520 nm of the visible spectrum of RR-P3HT.[31] For all of the P3HT oligomers, the $S_0 \rightarrow S_1$ transition is dominated by promotion of the HOMO to the LUMO.

The SLR calculations show that the exciton states ($S_1$) of P3HT oligomers with 6, 8, and 10 units absorb photons with wavelengths close to 900 nm. The ESA of P3HT-10 has the best agreement with experimental data. The dominant exciton absorption transitions are $S_1 \rightarrow S_5$ for $n = 10$, and $S_1 \rightarrow S_4$ for $n = 8$ and $n = 6$. None of these oligomers ($n = 6, 8, 10$) shows a strong absorption at 700 nm. This confirms the peak assignments of Guo et al.[30] and supports that the 700 nm band does not arise from exciton absorption, but a different species.

We denote for simplicity HOMO and LUMO as H and L, respectively. For P3HT-8, the $S_4$ state is characterized by four dominant single orbital transitions with respect to the ground state: H−2 → L+1, H−1 → L, H−1 → L+2, and H → L+1. In contrast, $S_5$ of P3HT-10 embodies mainly a H → L+1 and a H−1 → L transition. Using these excitations from the ground state as reference, we interpret the $S_1 \rightarrow S_4$ transition includes: a de-excitation from the LUMO (which is occupied in the $S_1$ state) back to the HOMO, then a promotion from the HOMO to partially populate L+1; and two excitations from levels below the HOMO to levels above the LUMO, whereas the $S_1 \rightarrow S_5$ excitation is L → L+1 and repopulation of the LUMO by the HOMO−1 level. Figure 2 visualizes the valence orbitals of
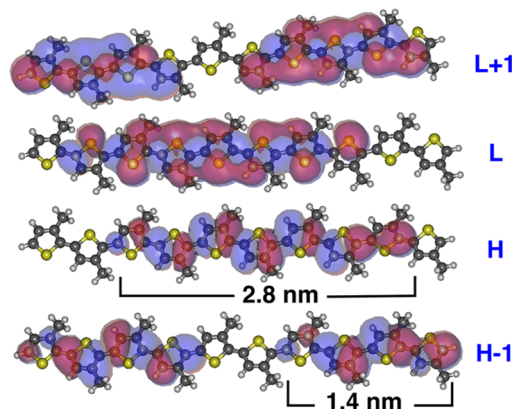


**Figure 2.** CAM-LDA0/cc-pVDZ isosurfaces (99% density confinement) of four orbitals involved in the exciton absorption of P3HT-10: H−1, H, L, and L+1. Atom colors: C, dark gray; S, yellow; H, light gray.

P3HT most commonly involved in the excitation processes. The shapes of these orbitals are consistent with the known nodal structures of P3HT molecular orbitals.

Figure 3 shows the result of the SLR calculations and experimental data reported by Hsu et al.[32] (dashed line). These authors performed photoluminescence (PL) and -absorption (PA) measurements in MEH-PPV films. The dashed line in
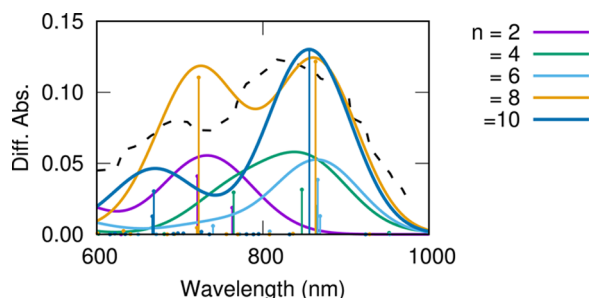
**Figure 3.** Calculated $S_1$ absorption spectra of MEH-PPV oligomers versus experimental exciton absorption data measured by Hsu et al.[32] on MEH-PPV films. Solid lines, SLR calculations; dashed line, experimental.

Figure 3 was recorded 200 ps after the excitation (at 600 nm). The PL spectra observed at 800 nm indicate that at 200 ps the excitons are a minority species. The PA at 800 nm requires fitting by two exponentials in the range between 0 and 500 ps after the excitation, one with time constant 10 ps, and the other with 1.2 ns. Because of noise, the fit only suggests the decay is biexponential, not that there is a process with 10 ps lifetime (the exciton lifetime is 300 ps). In addition, in Figure S2 we include data reported by Yan et al.[33] (●) and Samuel et al.[34] (+) for MEH-PPV (the spectra in dashed lines and ● were scaled for comparison with + symbols). The spectrum by Yan et al.[33] was taken immediately after the pump pulse (0 ps delay). The data measured by Samuel et al.[34] also display a similar absorption profile at 5 ps after an excitation at 315 nm. The slow exponential decay measured by Samuel et al.[34] for ESA at 800 nm agrees with the data of Hsu et al.[32] within 0.1 ps.

According to the SLR calculations, for all of the computed oligomers, except the one with two units, the excitons strongly absorb at wavelengths around 850 nm, in excellent agreement with the data reported by Hsu et al.[32] Only the excitons of oligomers with 8 and 10 units absorb near 700 nm. Absorption at this wavelength is responsible for the small shoulder of the spectrum shown in black circles, Figure 3. These results imply the transient absorption of the excitonic states and the bipolarons overlap, causing the biexponential decay of the spectral lines.

The main transitions are around 850 nm, $S_1 \rightarrow S_6$ and $S_1 \rightarrow S_7$ in oligomer MEH-PPV-8 and -10, respectively; around 750 nm, $S_1 \rightarrow S_{11}$ in MEH-PPV-8, whereas in MEH-PPV-10 it is a combination of separate transitions from $S_1$ to $S_{13}$, $S_{14}$, and $S_{15}$. Interestingly, the transitions peaking at 850 nm of MEH-PPV-8 and -10 are similar in character. With reference to the ground state, the $S_1$ state in both oligomers is dominated by H → L and H−1 → L+1, while in $S_6$ and $S_7$ there are four single particle transitions: H → L+1, H−1 → L, H−1 → L+2, and H−2 → L+1. Thus, the redistribution of the LUMO and LUMO+1 levels (Figure S7) in excitations from $S_1$ in both oligomers is similar for the absorption around 850 nm. The characters of the singlet transitions around 750 nm involve collectively many single-particle transitions, especially in MEH-PPV-10. In MEH-PPV-8, the orbital excitation with largest transition strength (maximum $X_{ai}$) is a H−9 → L promotion.

Last, we show the results of the SLR computations for PTB7 oligomers with 1, 2, and 3 units, Figure 4b. PTB7 is somewhat unique in that it is considered a donor−acceptor "charge-transfer" polymer, and potentially exhibits qualitatively different
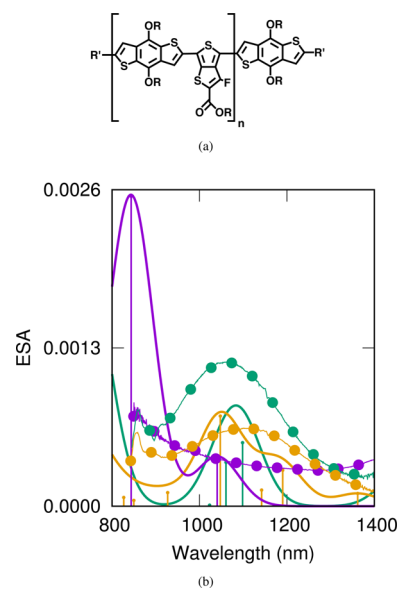


**Figure 4.** (a) Molecular formula of the oligomers studied experimentally, where R is TIPS-(triisopropylsilyl group), and R′ is ethylhexyl. (b) Calculated $S_1$ absorption spectra of PTB7-1 (purple), -2 (green), and -3 (gold). The experimental data are shown in lines and points (linespoints) for PTB7-1 (purple), -2 (green), and -3 (gold). For PTB7-2 and -3, the pump−probe delay is 200 ps, whereas for PTB7-1 it is 2 ps.

photophysics from P3HT and MEH-PPV.[35] We include transient absorption measurements taken at 200 ps after the pump perturbation for PTB7-2 and -3, and 2.5 ps for PTB7-1. Note that there is an extra aromatic monomer outside the bracket in Figure 4a; this unit does not affect significantly the experiment versus theory comparison. The pump−probe delays were chosen because of a difference in dynamics between the long and short oligomers: In the 2 and 3 unit oligomers, there is a fast-decay small component near 860 nm with a lifetime of 10 ps. The 200 ps delay was chosen to more accurately represent the singlet exciton without contribution of this faster decaying species. The initial excitation is at 540 nm, with pulse duration of 60 fs; the solvent used is chloroform. For PTB7-2 and PTB7-3, we note that there are two absorption bands: one broad band around 1100 nm and a thinner peak around 850 nm. On the other hand, PTB7-1 shows absorption around 850 nm, and no broad band around 1100 nm.

The computed ESA spectra for PTB7-2 and PTB7-3 indicate absorption near the two measured absorption bands, in agreement with the experiment. For PTB7-1 the SLR computations suggest that the band around 850 nm ($S_1 \rightarrow S_5$) is dominant over the small peak near 1050 nm, while no peak is visible in the experimental data within the range. In PTB7-2, the peak at 1098 nm ($S_1 \rightarrow S_5$) and its shoulder on the left are split into three smaller bands in PTB7-3, located at 1050 ($S_1 \rightarrow S_7$), 1190 ($S_1 \rightarrow S_5$), and 1361 nm ($S_1 \rightarrow S_4$). The experiment indicates a similar trend, that the band of PTB7-3 is broader than that of PTB7-2. However, the net shift of the broad bands in the experiment (from left to right) is not fully captured by the calculations: The tallest peak of PTB7-3 is at 1050 nm, while for PTB7-2 it is 1098 nm. We believe this is caused by in-solution structural dynamics of equilibrium states (and excited states, when pump−probe delays are significant) of the oligomers, not considered in this calculation, and/or errors due to the functional and basis set used. We ran CAM-

PBE0 calculations and noted that, even though the shift of oscillator strengths (Figure S3) displays some improvement, the accuracy in the relative heights and positioning of the peaks is reduced with respect to CAM-LDA0 results. Alternatively, double-hybrid approaches,[36] which include (in addition to nonlocal exchange) nonlocal elements in the correlation energy, might offer further improvements, but they require new extensions to conventional LR algorithms that can potentially increase the computational scaling.

In PTB7-1, the tallest peak shown in the plot is a $S_1 \rightarrow S_5$ excitation. With respect to the $S_1$ state (roughly speaking), the LUMO electrons are promoted to LUMO+2, and the pair in the HOMO−4 reoccupies the LUMO. Furthermore, the states $S_5$ and $S_7$ of PTB7-2 and -3, respectively, show some common single-orbital excitations (Table 1, Figure 5). The excitation

**Table 1. First Four Dominant Orbital Transitions (Taken from the First LR TDDFT Calculations) in the $S_5$ and $S_7$ States of PTB7-2 and -3**

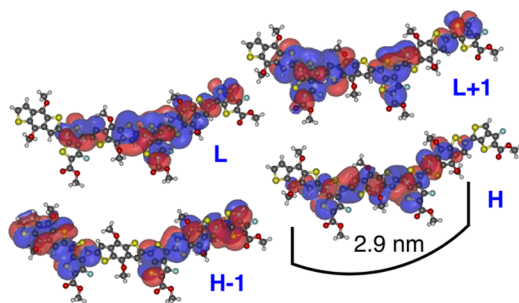| PTB7-2 | | PTB7-3 | |
| --- | --- | --- | --- |
| $S_5$ | $S_7$ | $S_5$ | $S_7$ |
| H−3 → L+1 | H−3 → L+1 | H−3 → L | H−4 → L |
| H−1 → L | H−3 → L+3 | H−3 → L+1 | H−3 → L+1 |
| H → L+1 | H−1 → L+3 | H−2 → L+1 | H−2 → L |
| H → L+2 | H → L+3 | H−1 → L | H → L+1 |



**Figure 5.** CAM-LDA0/cc-pVDZ orbital surfaces (99% density confinement) of the levels H−1, H, L, and L+1, of the oligomer PTB7-3. Additional atom colors: O, red; F, light blue.

H−3 → L+1 is present in all four singlet states included in Table 1, whereas the $S_5$ states of PTB7-2 and -3 also share the H−1 → L transition. The donor−acceptor nature of PTB7 molecular orbitals is evidenced by the localized nature of the LUMO orbitals relative to those of P3HT. The H−1 and L−1 orbital distribution is clearly more inhomogeneous than the P3HT H−1 and L−1 orbitals, which supports our previous statement of vital differences in torsional degrees of freedom of PTB7. It is likely that this combination of torsional disorder and donor−acceptor-induced charge-transfer character is a significant cause behind the errors involved in the PTB7 calculation, which we attributed to geometric relaxation and functional deficiencies.

Summarizing the results of P3HT and MEH-PPV, the molecular orbitals mediating ESA in conjugated polymers are often H/L → H−1/L and H/L → H/L+1 in character, where A/B denotes transition from orbital A to B, originating at the ground state. In the long oligomer limit of P3HT, $S_1 \rightarrow S_5$ is the dominant transition exhibiting this character, and for MEH-PPV, $S_1 \rightarrow S_6$ and $S_1 \rightarrow S_7$ show significant tendencies toward this orbital character. This characterization of the dominant

contributing orbitals is supported by previous theoretical work on the homopolymer polyfluorene,[3,4,37] with one study usefully describing the orbital character of the low-energy near-IR transitions as being exactly H/L → H−1/L and H/L → H/L +1,[3] as observed in this work for P3HT and MEH-PPV.

In the case of homopolymers, these orbital contributions suggest a simple rule-of-thumb for predicting peak positions of singlet exciton absorptions in conjugated polymers: as a zeroth-order approximation, one can assume the dominant oscillator strength transition is H/L → H−1/L and H/L → H/L+1 in character, identify the lowest lying singlet excitation with H/L character, and the single excitation in the rough near-IR region with primarily H−1/L and H/L+1 character. The energy difference between these two singlet excited states should roughly correspond to the excited-state absorption energy observed spectrally.

We observe the SLR calculations miss expected peaks in the tail (beyond 1000 nm) of the experimental P3HT ESA spectrum. These missing states need a description that considers long (flexible) polymeric chains, interaction with neighbors, and molecular motion leading to peak broadening. Capturing bulk and solvent effects are additional challenges of high relevance for future work. We believe a careful combination of classical MD with SLR might help as the initial step in elucidating these effects. It would be desirable to use fully ab initio periodic calculations for these type of problems. However, the high cost of computing quantities such as nonlocal Hartree−Fock exchange could make this task difficult. There is promise in methods[38] developed to partition quantum mechanical systems into a system and a bath (so both are treated by quantum mechanics), and these could easily help SLR methods afford more realistic descriptions.

Despite that the SLR computations costs match those of regular LR TDDFT, preferred robust functionals with Coulomb attenuation (or range separation) remain more expensive than more affordable functionals such as PBE or BLYP. Here, the inclusion of exact exchange and its long-range form using the error function is also responsible for this increase in computational demands, but it offers better accuracy in excitation energies (which is essential for the quality of excited state−excited state transition energies, especially for large oligomers). This is a significant limitation for application in periodic systems. Fortunately, research to eliminate this limitation is progressing.[39]

The SLR method could be used to study the formation of other transient species such as (bi)polarons, excimers, and charge-transfer states. There are two cases: (i) The transient species geometry is known and lies in an excited state. (ii) The SLR theory is used to design new methods to calculate nonadiabatic couplings and then applied to predict the conversion of transient species into others. For example, in case (i), the experimentalist could hypothesize that a singlet excited state transformed into an excited triplet and could use SLR to calculate its absorption spectrum and confirm her/his assumption. In case (ii), the calculation of nonadiabatic elements involving nuclear gradients may also proceed in analogy with standard LR,[40] through pole analysis of averaged nuclear gradients (over electronic degrees of freedom), where the initial states are perturbed as suggested in this Article. In this direction, the SLR method provides new routes to predict the formation of transient species.

## ■ CONCLUSION

Motivated by the challenge of reducing the computational scaling, and improving the accuracy of theories describing excited-state phenomena, we showed that our second linear response TDDFT methodology based on wave function theory can efficiently calculate exciton absorption spectra of a wide set of oligomers of P3HT, MEH-PPV, and PTB7. The calculations are consistent with transient experimental data for the three types of materials explored. For P3HT and MEH-PPV, we observe that the red-most absorption bands converge around 10 monomer units, whereas for the PTB7 oligomers studied here our model identifies the near-IR bands of the excitonic states. With regard to MEH-PPV, the computations confirm that the exciton absorption overlaps with the signal corresponding to the ultrafast formation of bipolarons. For future work, we believe it important to develop new time-dependent XC potentials that can improve the quality of excited-state spectra, with reduced computational cost. Furthermore, work on applications to describe the formation of other species like bipolarons, and on speeding traditional LR TDDFT calculations, is in progress.

## ■ ASSOCIATED CONTENT

### Ⓢ Supporting Information

The Supporting Information is available free of charge on the ACS Publications website at DOI: 10.1021/jacs.6b12405.

> Complementary ESA spectra, molecular drawings, orbitals, and computed oscillator strengths of the $S_1$ excited states (PDF)
>
> All computed molecule Cartesian coordinates (XYZ)

## ■ AUTHOR INFORMATION

### Corresponding Author
*ratner@northwestern.edu

### ORCID Ⓘ
Martín A. Mosquera: 0000-0003-2170-5651
Nicholas E. Jackson: 0000-0002-1470-1903

### Notes
The authors declare no competing financial interest.

## ■ ACKNOWLEDGMENTS

## ■ REFERENCES

(1) Reid, O. G.; Pensack, R. D.; Song, Y.; Scholes, G. D.; Rumbles, G. *Chem. Mater.* **2014**, *26*, 561−575.

(2) Savoie, B. M.; Jackson, N. E.; Chen, L. X.; Marks, T. J.; Ratner, M. A. *Acc. Chem. Res.* **2014**, *47*, 3385−3394.

(3) Ling, S.; Schumacher, S.; Galbraith, I.; Paterson, M. J. *J. Phys. Chem. C* **2013**, *117*, 6889−6895.

(4) Fischer, S. A.; Cramer, C. J.; Govind, N. *J. Chem. Theory Comput.* **2015**, *11*, 4294−4303.

(5) De Giovannini, U.; Brunetto, G.; Castro, A.; Walkenhorst, J.; Rubio, A. *ChemPhysChem* **2013**, *14*, 1363−1376.

(6) Zhao, Y.; Truhlar, D. G. *Acc. Chem. Res.* **2008**, *41*, 157−167.

(7) Tao, J.; Perdew, J. P.; Staroverov, V. N.; Scuseria, G. E. *Phys. Rev. Lett.* **2003**, *91*, 146401.

(8) Casida, M. E.; Huix-Rotllant, M. In *Density-Functional Methods for Excited States*; Ferré, N., Filatov, M., Hiux-Rotllant, M., Eds.; Springer: Switzerland, 2015; pp 1−60.

(9) Wagner, L. O.; Yang, Z.-h.; Burke, K. In *Fundamentals of Time-Dependent Density Functional Theory*; Marques, M. A. L., Maitra, N. T., Nogueira, F. M. S., Gross, E. K. U., Rubio, A., Eds.; Springer: New York, 2012; pp 101−123.

(10) Sałek, P.; Vahtras, O.; Helgaker, T.; Ågren, H. *J. Chem. Phys.* **2002**, *117*, 9630−9645.

(11) Cronstrand, P.; Christiansen, O.; Norman, P.; Agren, H. *Phys. Chem. Chem. Phys.* **2000**, *2*, 5357−5363.

(12) Hettema, H.; Jensen, H. J. A.; Jørgensen, P.; Olsen, J. *J. Chem. Phys.* **1992**, *97*, 1174−1190.

(13) Isborn, C. M.; Li, X. *J. Chem. Phys.* **2008**, *129*, 204107.

(14) Provorse, M. R.; Habenicht, B. F.; Isborn, C. M. *J. Chem. Theory Comput.* **2015**, *11*, 4791−4802.

(15) Provorse, M. R.; Isborn, C. M. *Int. J. Quantum Chem.* **2016**, *116*, 739−749.

(16) Luo, K.; Fuks, J. I.; Maitra, N. T. *J. Chem. Phys.* **2016**, *145*, 044101.

(17) Mosquera, M. A.; Chen, L. X.; Ratner, M. A.; Schatz, G. C. *J. Chem. Phys.* **2016**, *144*, 204105.

(18) Perdew, J. P.; Burke, K.; Ernzerhof, M. *Phys. Rev. Lett.* **1996**, *77*, 3865.

(19) (a) Hariharan, P. C.; Pople, J. A. *Theor. Chem. Acc.* **1973**, *28*, 213−222. (b) Francl, M. M.; Pietro, W. J.; Hehre, W. J.; Binkley, J. S.; Gordon, M. S.; DeFrees, D. J.; Pople, J. A. *J. Chem. Phys.* **1982**, *77*, 3654−3665.

(20) Risko, C.; McGehee, M. D.; Brédas, J.-L. *Chem. Sci.* **2011**, *2*, 1200−1218.

(21) (a) Dirac, P. A. *Note on Exchange Phenomena in the Thomas Atom*; Math. Proc. Cambridge Philos. Soc., 1930; pp 376−385. (b) Slater, J. C. *Adv. Quantum Chem.* **1972**, *6*, 1−92.

(22) Vosko, S. H.; Wilk, L.; Nusair, M. *Can. J. Phys.* **1980**, *58*, 1200−1211.

(23) Yanai, T.; Tew, D. P.; Handy, N. C. *Chem. Phys. Lett.* **2004**, *393*, 51−57.

(24) (a) Kim, K.; Jordan, K. *J. Phys. Chem.* **1994**, *98*, 10089−10094. (b) Becke, A. D. *Phys. Rev. A: At., Mol., Opt. Phys.* **1988**, *38*, 3098. (c) Lee, C.; Yang, W.; Parr, R. G. *Phys. Rev. B: Condens. Matter Mater. Phys.* **1988**, *37*, 785.

(25) Rohrdanz, M. A.; Herbert, J. M. *J. Chem. Phys.* **2008**, *129*, 034107.

(26) Mosquera, M. A.; Borca, C. H.; Ratner, M. A.; Schatz, G. C. *J. Phys. Chem. A* **2016**, *120*, 1605−1612.

(27) (a) Dunning, T. H., Jr *J. Chem. Phys.* **1989**, *90*, 1007−1023. (b) Woon, D. E.; Dunning, T. H., Jr *J. Chem. Phys.* **1993**, *98*, 1358−1371.

(28) (a) Binkley, J. S.; Pople, J. A.; Hehre, W. J. *J. Am. Chem. Soc.* **1980**, *102*, 939−947. (b) Stevens, W. J.; Basch, H.; Krauss, M. *J. Chem. Phys.* **1984**, *81*, 6026−6033. (c) Stevens, W. J.; Krauss, M.; Basch, H.; Jasien, P. G. *Can. J. Chem.* **1992**, *70*, 612−630.

(29) Valiev, M.; Bylaska, E. J.; Govind, N.; Kowalski, K.; Straatsma, T. P.; Van Dam, H. J. J.; Wang, D.; Nieplocha, J.; Apra, E.; Windus, T. L.; Jong, W. A. *Comput. Phys. Commun.* **2010**, *181*, 1477−1489.

(30) Guo, J.; Ohkita, H.; Benten, H.; Ito, S. *J. Am. Chem. Soc.* **2009**, *131*, 16869−16880.

(31) Manceau, M.; Chambon, S.; Rivaton, A.; Gardette, J.-L.; Guillerez, S.; Lemaître, N. *Sol. Energy Mater. Sol. Cells* **2010**, *94*, 1572−1577.

(32) Hsu, J.; Yan, M.; Jedju, T.; Rothberg, L.; Hsieh, B. *Phys. Rev. B: Condens. Matter Mater. Phys.* **1994**, *49*, 712.

(33) Yan, M.; Rothberg, L.; Kwock, E.; Miller, T. *Phys. Rev. Lett.* **1995**, *75*, 1992.

(34) Samuel, I.; Raksi, F.; Bradley, D.; Friend, R.; Burn, P.; Holmes, A.; Murata, H.; Tsutsui, T.; Saito, S. *Synth. Met.* **1993**, *55*, 15−21.

(35) Rolczynski, B. S.; Szarko, J. M.; Son, H. J.; Liang, Y.; Yu, L.; Chen, L. X. *J. Am. Chem. Soc.* **2012**, *134*, 4142−4152.

(36) Grimme, S.; Neese, F. *J. Chem. Phys.* **2007**, *127*, 154116.

(37) Pandey, L.; Doiron, C.; Sears, J. S.; Brédas, J.-L. *Phys. Chem. Chem. Phys.* **2012**, *14*, 14243−14248.

(38) (a) Neugebauer, J. *Phys. Rep.* **2010**, *489*, 1−87. (b) Pavanello, M. *J. Chem. Phys.* **2013**, *138*, 204118. (c) Jacob, C. R.; Neugebauer, J. *Wiley Interdiscip Rev. Comput. Mol. Sci.* **2014**, *4*, 325−362.

(39) Lin, L. *J. Chem. Theory Comput.* **2016**, *12*, 2242−2249.

(40) Send, R.; Furche, F. *J. Chem. Phys.* **2010**, *132*, 044107.